THE JOURNAL OF PHYSICAL CHEMISTRY B
A JOURNAL OF THE AMERICAN CHEMICAL SOCIETY

pubs.acs.org/JPCB

Article

Refinement of the Optimized Potentials for Liquid Simulations Force Field for Thermodynamics and Dynamics of Liquid Alkanes

Mohammad M. Ghahremanpour, Julian Tirado-Rives, and William L. Jorgensen*

Cite This: *J. Phys. Chem. B* 2022, 126, 5896−5907

Read Online

ACCESS | Metrics & More | Article Recommendations

ABSTRACT: Torsion and Lennard-Jones parameters of the optimized potentials for liquid simulations (OPLS) all-atom force field have been refined for describing thermodynamics and dynamics of a wide range of liquid alkanes. Monte Carlo statistical mechanics (MC) and molecular dynamics (MD) simulations were carried out. For thermodynamics properties, MC simulations with truncated electrostatic interactions performed very closely to MD simulations with a Verlet neighbor list and the particle mesh Ewald algorithm. The average errors in comparison with experimental data for computed properties were improved with the modified force field (OPLS/2020), especially for long-chain alkanes. For liquid densities, heats of vaporization, and free energies of hydration, the average errors are 0.01 g/cm^3, 0.2 kcal/mol, and *ca.* 0.5 kcal/mol, respectively; significant gains were made for relative heats of vaporization of isomeric series. Results for self-diffusion coefficients also reproduce experimental data well for linear alkane liquids up to hexadecane. The new force field is suitable for use in improved modeling of myriad systems of importance in chemistry, biology, and materials science.

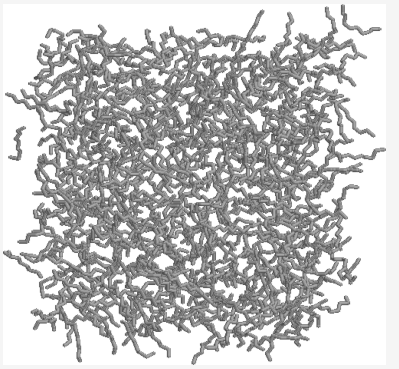

1. INTRODUCTION

Steady progress has been made in the development of molecular-mechanics force fields for modeling hydrocarbons in both the gas and the liquid phase over the past 50 years.[1−13] Accurate description of the properties of the wide range of short, long, linear, cyclic, unbranched, branched, and strained hydrocarbons with a single set of force-field parameters has remained challenging. In early efforts, crystal structures, gas-phase thermochemistry, and molecular vibrational frequencies were key items used as the basis of parameterization.[1,4] However, the most common application of molecular simulations is to study chemical phenomena in the liquid phase, but computer simulations of other than simple liquids were uncommon before 1980. With advances in computer resources and development of appropriate software, the original optimized potentials for liquid simulations (OPLS), in addition to considering gas-phase structures and conformational energetics, began the now-common practice of refinement of force-field parameters by iterative simulations of organic liquids.[3] The reproduction of observed densities and heats of vaporization was emphasized with some attention also given to heat capacities and isothermal compressibilities. For hydrocarbons, the force field began using a united-atom model (OPLS-UA) with hydrogen atoms implicit[3] and was subsequently advanced to the all-atom model, OPLS-AA.[5,6] However, the original testing was for small alkanes, alkenes, and substituted benzenes with mostly no more than six carbon atoms.[3,5,6] A subsequent study of alkanes with up to 12 carbon atoms revealed a pattern of increasing overestimation of heats of vaporization with increasing chain length and a likely overestimation of *gauche-anti* energy differences leading to too-low populations of *gauche*-containing conformers.[11] The latter issue was also noted in the development of alternative force fields and resulted in the downward revision of the *gauche-anti* energy difference for butane and other C−C−C−C torsions from *ca.* 0.9 to 0.6 kcal/mol.[10] This has led to better performance for systems containing longer hydrocarbon chains including lipid bilayers.[10,14,15] In particular, diffusivity and melting points can be improved, and improper liquid-gel phase transitions can be eliminated.[10,14,15]

As another issue, the previous work on OPLS force fields for hydrocarbons was largely based on the results of Monte Carlo (MC) simulations and consequently did not consider transport properties that require molecular dynamics (MD). Although computation of self-diffusion coefficients played a role in the development of water models,[16] their computation for organic liquids, especially for flexible chains as in longer alkanes, is more computationally challenging. The slow equilibration and variation of conformational degrees of freedom in such systems contribute to slow convergence.[17] Rotations about C−C bonds

Received: May 28, 2022
Revised: July 18, 2022
Published: August 1, 2022

in a hydrocarbon chain are not independent because of van der Waals contacts between non-neighboring groups, and the inter-chain contacts also retard conformational sampling. The populations of the *gauche* and *anti* conformations and the strength of van der Waals interactions are, therefore, important in regulating the packing and fluidity of liquid hydrocarbons. Fortunately, the increase in computing power and the advances in parallel execution of molecular dynamics programs have made it practical to systematically validate force fields on the transport properties of organic liquids.

Thus, the present refinement of the OPLS-AA force field for alkanes was primarily motivated to address the prior deficiencies in the treatment of longer alkanes to include calculation of transport properties and to provide testing on a larger selection of both linear and branched alkanes. Deficiencies in the ordering and range of computed heats of vaporization for isomers are also noted and improved upon. The new hydrocarbon parameters presented here are part of the OPLS/2020 force field, which has also addressed the treatment of cation-π interactions in a formally nonpolarizable force field.[18] The opportunity has also been taken to make a complete presentation for all current force-field parameters for calculations on alkanes in one place. Our emphasis was on modeling a wide range of alkanes at 1 atm pressure near room temperature or at their boiling points with some exploration of other conditions; results are reported for 25 liquid alkanes. The importance of accurate force fields for modeling hydrocarbons cannot be overstated because they form the underpinnings for simulations of organic and biomolecular systems, and they also receive extensive application in materials, petroleum, atmospheric, and prebiotic science.

2. COMPUTATIONAL DETAILS

2.1. Monte Carlo. All Metropolis MC simulations were carried using the BOSS program[19] using established procedures.[11] In both gas- and liquid-phase simulations, all internal degrees of freedom were sampled. A random set of bond lengths, bond angles, and dihedral angles is chosen for variation upon an MC move. The ranges are set automatically by the program; they are *ca.* ±0.03 Å for bond lengths, ±5° for bond angles, ±15° for principal torsions, and ±2° for improper dihedral angles. The default, which was used here, is to vary a maximum of 15 internal degrees of freedom of each type. The MC simulations of the pure alkane liquids were carried out in the *NPT* ensemble at 25 °C or at the boiling point of the liquid and 1 atm with Metropolis sampling of all internal and intermolecular degrees of freedom. In each case, a cubic, periodic box of 500 monomers was generated and force-field cutoffs of 12 Å were used, along with quadratic smoothing and a standard correction for the Lennard-Jones (LJ) interactions neglected beyond the cutoff.[3] If any C−C distance between two molecules is within the cutoff, the entire molecule-molecule interaction is included in the total energy. The *NPT* simulations included attempts to alter the volume every 3125 configurations. Initial coordinates are generated using an algorithm in BOSS that centers the monomers at the atomic positions in a cube of liquid argon that is expanded to *ca.* 80% of the expected final density. Each liquid was first equilibrated for at least 25×10^6 configurations, and averaging took place over at least 25×10^6 configurations. For heptane through decane, these periods were both increased to at least 50×10^6 configurations. In all cases, the total energy and volume were well converged after the equilibration period. However, the MC simulation for liquid dodecane was still drifting slowly in energy after 125×10^6 configurations, so only MD results are reported for it and larger alkanes.

Absolute free energies of hydration (ΔG_{aq}) were also computed with MC simulations using free energy perturbation (FEP) theory for nine molecules. All aqueous simulations were performed using standard protocols[20] in the *NPT* ensemble at 25 °C and 1 atm in a periodic cube, *ca.* 25 Å on an edge, containing 500 TIP*n*P (n = 3, 4, 5) water molecules.[16,19] Fifteen windows of simple overlap sampling were applied with 3×10^6 configurations of equilibration and at least 15×10^6 configurations of averaging in each window.[20] All solvent−solvent and solute−solvent intermolecular interactions were truncated at 10 Å with quadratic smoothing over the last 0.5 Å and with a cutoff correction as above. Molecules were perturbed to homologs, while methane was perturbed to a null particle. FEP calculations were performed in the gas and aqueous phases with the difference in results yielding the $\Delta\Delta G_{aq}$, which were summed and anchored to the result for methane to give ΔG_{aq}.[20]

2.2. Molecular Dynamics. All MD simulations were carried out with the GROMACS program (version 2019).[21] In the gas-phase simulations, a leap-frog algorithm adopted for stochastic dynamics (SD) was used because SD integrators add a friction term to the equations of motion that reduces the accumulation of errors for the rotational and translational degrees of freedom when a system is simulated in a vacuum. This makes sampling of different configurations more efficient.

The Packmol[22] software was used to randomly place 512 molecules in a cubic box with a distance tolerance of 2.0 Å for every pair of atoms of different molecules. Energy minimization was performed on the initial liquid configuration until the steepest descent algorithm converged to a maximum force smaller than 2.4 kcal mol^{-1} $Å^{-1}$. An initial velocity was sampled, for each atom, from a Maxwell−Boltzmann distribution at 25 °C or at the boiling point temperature of the liquid. Subsequently, each system was equilibrated for 500 ps in the *NVT* ensemble under periodic boundary conditions. The v-rescale thermostat with a stochastic term was used to maintain the temperature at the desired value.[23] The stochastic term ensured that the sampled ensemble was canonical. The coupling constant of the thermostat was set to 2.0 ps. Each liquid was then equilibrated for 2.0 ns in the *NPT* ensemble to obtain a density consistent with the reference pressure of 1 atm. The Berendsen barostat was used in the equilibration phase with a compressibility factor of 4.5×10^{-5} bar.[24] Finally, the *NPT* ensemble was sampled for each system for 10 ns using the Parrinello−Rahman barostat.[25] The coupling constant of both barostats was set to 4.0 ps. All steps were repeated three times for each alkane to check the reproducibility of the results.

A buffered Verlet neighbor list of 12 Å was generated every 10 integration steps for evaluating nonbonded interactions.[26] The LJ forces were smoothly decreased to zero between 10 and 12 Å. Analytical long-range dispersion corrections were applied to instantaneous energies and pressures. Two simulation protocols were applied based on the treatment of electrostatic interactions. In setup 1, denoted by MD-Cutoff, electrostatic interactions were only calculated within a cutoff of 12 Å. In setup 2, denoted by MD-PME, electrostatic interactions beyond the cutoff radius were also included using the particle mesh Ewald (PME) algorithm[27] with an interpolation order of 6, a relative tolerance of 10^{-6}, and a

https://doi.org/10.1021/acs.jpcb.2c03686
J. Phys. Chem. B 2022, 126, 5896−5907

Fourier spacing of 1.2 Å. The LINCS algorithm[28] was used to constrain covalent bonds to hydrogens in all alkanes, except for cyclopropane, cyclobutane, and cyclopentane, where all covalent bonds were constrained to avoid instability of the simulations. The interpolation order of LINCS was set to 12.

The hydration free energies were calculated using free energy perturbation calculations. Equilibrated boxes of 1000 TIP*n*P (n = 3, 4, 5)[16,29] water molecules were used for solvating the alkanes. The λ schedule for calculating the hydration free energy in this work has 20 windows. The first five windows decouple the Coulombic interactions, while the last 15 windows decouple the LJ interactions between the solute and the solvent molecules. A soft-core (SC) potential was applied to alleviate issues because of strong LJ interactions. The SC-power and SC-sigma parameters were set to 1.0 and 0.5, respectively. A Langevin integrator was used with a time step of 1 fs. Each system was equilibrated for 1 ns using the *NVT* ensemble followed by 1 ns equilibration using the *NPT* ensemble for each λ window. Production simulations were then performed for 5 ns using the *NPT* ensemble. The hydration free energy was estimated by exponential averaging of the potential energy differences between the initial state (λ_i) and the final state (λ_f) during the production simulations using the alchemical-analysis Python script.[30]

2.3. Calculation of Properties of Pure Liquids. The enthalpy of vaporization was computed from eq 1, where $\langle ... \rangle$ denotes an ensemble average, E_{pot} is the

$$\Delta H_{vap} = \langle E_{pot} \rangle_g - \langle E_{pot} \rangle_l + RT \tag{1}$$

potential energy, R is the ideal gas constant, and T is the absolute temperature. In a liquid simulation at constant pressure, the density is the mass M of the system divided by the volume V (eq 2).

$$\rho = \frac{M}{\langle V \rangle} \tag{2}$$

The coefficient of isothermal compressibility of the liquid alkanes is calculated from the fluctuations in their volume during Monte Carlo simulations (eq 3), where k_β is the Boltzmann constant. The heat capacity at constant pressure for the

$$\kappa = \frac{1}{k_\beta T} \frac{\langle \delta V^2 \rangle}{\langle V \rangle} \tag{3}$$

the liquid, $C_p(l)$, is calculated from Monte Carlo simulations using eq 4, where C_p^o is

$$C_p(l) = \frac{\langle \delta H^2 \rangle}{k_\beta T^2} \approx C_p^o + C_p(\text{inter}) - R \tag{4}$$

the experimental heat capacity for the ideal gas, and C_p(inter) is calculated from the fluctuations of the total intermolecular energy during the MC simulations.

The self-diffusion coefficient for the liquid alkanes is calculated from the MD simulations by fitting a straight line to the mean-square displacement (MSD) of the centers of masses of molecules simulated under the periodic boundary conditions (PBC) using the Einstein relation (eq 5), where r_i is the position of the center of mass

$$D_{PBC} = \frac{1}{6} \lim_{t \to \infty} \frac{d}{dt} \langle |r_i(t) - r_i(0)|^2 \rangle \tag{5}$$

of molecule i. The system-size dependence of D_{PBC}, which is an artifact of the periodic boundary conditions, can be analytically corrected using the formula in eq 6,

$$D_0 = D_{PBC} + \frac{k_\beta T \xi}{6\pi\eta L} \tag{6}$$

where η is the shear viscosity of the liquid, L is the length of the simulation box, and ξ is a constant that equals 2.837298 for the cubic lattice symmetry.[17,31] The correction is in principle like the Stokes−Einstein relation for the diffusion of spherical particles through a liquid.

3. RESULTS AND DISCUSSION

3.1. OPLS/2020 Parameters. The form of the force field is unchanged and given in eqs 7−10, which represent the bond-stretching, angle-bending, torsional,

Table 1. OPLS/2020 Nonbonded Parameters for Alkanes[a]

		OPLS-AA		OPLS/2020	
atom	q	σ	ε	σ	ε
H	0.06	2.500	0.030	**2.480**	**0.026**
C in					
CH_4	−0.24	3.500	0.066	**3.570**	**0.060**
n-CH_3	−0.18	3.500	0.066	**3.550**	0.066
iso-CH_3	−0.18	3.500	0.066	**3.400**	**0.072**
neo-CH_3	−0.18	3.500	0.066	**3.340**	**0.070**
CH_2	−0.12	3.500	0.066	**3.510**	0.066
CH	−0.06	3.500	0.066	3.500	0.066
C	0.00	3.500	0.066	3.500	0.066
CH_2 (*c*-C_3)[b]	−0.12	3.500	0.066	**3.430**	**0.088**
CH (*c*-C_3)[b]	−0.06	3.500	0.066	**3.430**	**0.088**
C (*c*-C_3)[b]	0.00	3.500	0.066	**3.430**	**0.088**
CH_2 (*c*-C_4)[c]	−0.12	3.500	0.066	**3.470**	**0.077**
CH (*c*-C_4)[c]	−0.06	3.500	0.066	**3.470**	**0.077**
C (*c*-C_4)[c]	0.00	3.500	0.066	**3.470**	**0.077**

[a]Parameters in bold are changed from OPLS-AA. LJ σ in Å; ε in kcal/mol. $R^* = 2^{1/6}(\sigma/2)$. [b]In cyclopropanes. [c]In cyclobutanes.

$$E_{bond} = \sum_b K_{r,b}(r - r_{eq})^2 \tag{7}$$

$$E_{angle} = \sum_a K_{\theta,a}(\theta - \theta_{eq})^2 \tag{8}$$

$$E_{torsion} = \frac{1}{2} \sum_t [V_{1,t}(1 + \cos\phi) + V_{2,t}(1 - \cos 2\phi) + V_{3,t}(1 + \cos 3\phi) + V_{4,t}(1 - \cos 4\phi)] \tag{9}$$

$$E_{ab} = \sum_i^{\in a} \sum_j^{\in b} \left[\frac{q_i q_j}{r_{ij}} e^2 + 4\varepsilon_{ij} \left(\frac{\sigma_{ij}^{12}}{r_{ij}^{12}} - \frac{\sigma_{ij}^{6}}{r_{ij}^{6}} \right) \right] f_{ij} \tag{10}$$

and nonbonded energies. The nonbonded interactions are evaluated for all intermolecular pairs of atoms in molecules, a and b, and intramolecular pairs separated by >3 bonds with f_{ij} = 1.0, and f_{ij} = 0.5 for all intramolecular pairs separated by 3 bonds. The combining rules for the LJ parameters are $\sigma_{ij} = (\sigma_{ii}\sigma_{jj})^{1/2}$ and $\varepsilon_{ij} = (\varepsilon_{ii}\varepsilon_{jj})^{1/2}$. The terms are summed to give the total energy of the system.

https://doi.org/10.1021/acs.jpcb.2c03686
J. Phys. Chem. B 2022, 126, 5896−5907

Table 2. OPLS/2020 Bond Stretching, Angle Bending, and Torsion Parameters[a]

stretch	r_{eq}		K_r
CT−CT	1.529		268
CT−HC	1.090		340
CY−CY	1.520		260
CT−CY	1.510		280
CY−HC	1.088		340
bend	θ_{eq}		K_θ
CT−CT−CT	112.7		58.35
CT−CT-HC	110.7		37.5
HC−CT−HC	107.8		33.0
CY−CT−HC	110.7		37.5
CY−CY−HC	117.2		37.5
CY−CY−CT	117.2		37.5
CY−CY−CY	83.0		30.0
CT−CY−CT	114.3		35.0
CT−CY−HC	114.3		35.0
HC−CY−HC	114.3		35.0
torsion	V_1	V_2	V_3
CT−CT−CT−CT	**0.85**	**−0.20**	0.20
CT−CT−CT−CT[b]	**1.10**	**−0.20**	0.20
CT−CT−CT-HC	0.0	0.0	0.30
HC−CT−CT-HC	0.0	0.0	0.30
??−CY−CY−??	0.0	0.0	0.0
CY−CY−CT−HC	0.0	0.0	0.30
CT−CY−CT−HC	0.0	0.0	0.30

[a]Parameters in **bold** are changed from OPLS-AA. r_{eq} in Å; K_r in kcal/mol Å^2; θ_{eq} in deg; K_θ in kcal/mol deg^2; V in kcal/mol; all $V_4 = 0$. CT and HC are alkane carbon and hydrogen, except CY is used for 3- and 4-membered rings. [b]Butane only.

Table 3. Relative Conformational Energies for Alkanes (kcal/mol)

molecule	conformers	"best QM"	OPLS-AA	OPLS/2020
ethane	*e*−*s*	2.90[a]	2.84	2.82
butane	*g*−*a*	0.60[b]	0.80	0.58
butane	120°-*a*	3.30[c]	3.23	3.04
butane	*cis*-*a*	5.20[c]	5.18	5.11
pentane	*ag*−*aa*	0.61[b]	0.94	0.52
pentane	*gg*−*aa*	0.96[b]	1.89	1.04
pentane	g^+g^-−*aa*	2.81[b]	3.29	2.51
hexane	*aag*−*aaa*	0.60[b]	0.93	0.51
hexane	*aga*−*aaa*	0.60[b]	1.05	0.60
hexane	*agg*−*aaa*	0.93[b]	1.97	1.10
hexane	*gag*−*aaa*	1.18[b]	1.82	0.97
hexane	*ggg*−*aaa*	1.25[b]	2.09	1.59
2,3-dimethylbutane	*g*−*a*	0.05[d]	−0.23	0.54
methylcyclohexane	ax−eq	1.76[e]	1.78	0.82
1,2-dimethylcyclohexane	*cis*-*trans*	1.81[f]	1.61	0.68
decalin	*cis*-*trans*	3.08[g]	2.96	1.66
cyclobutane	D_{4h}−D_{2d}	1.46[h]	1.55	1.63
methylcyclobutane	ax−eq	0.71[i]	0.54	0.43
cyclohexane	tb−chair	5.98[j]	7.01	7.02
cycloheptane	b−tc	3.30[k]	4.75	4.57
cyclooctane	D_{4d}−C_s	2.00[k]	−1.04	−0.78
octadecane	linear−turn	1.0[l]	−1.34	0.55

[a]Ref 33. [b]Ref 32. [c]Ref 10. [d]Ref 34. [e]Ref 35. [f]Ref 36. [g]Ref 37. [h]Ref 38. [i]Ref 39. [j]Ref 40. [k]Ref 41. [l]Ref 42.

The alkane parameters for OPLS/2020 were modified as little as possible from OPLS-AA; they were derived from iterative MC simulations to reduce the error in the calculated properties of liquid alkanes and to obtain good gas-phase conformational energetics. The new and old nonbonded parameters are given in Table 1. Atomic partial charges were not modified because the magnitudes are small and small changes have little impact and were not found to be beneficial.[5,7] The biggest difference is the use of three types of methyl groups as in OPLS-UA,[3] depending on the adjacent branching as opposed to only one type with OPLS-AA. This was needed to obtain significant improvements in computed densities and heats of vaporization, especially for alkane isomers, as discussed below. There is a decrease in σ and increase in ε in progressing from methane to primary to secondary to tertiary methyl groups. It also means that for protein force fields, improvements can be expected by treating methyl groups differently as in homoalanine (AABA), alanine, and α-aminoisobutyric acid (AIB) residues. The LJ parameters for alkane hydrogen atoms have also been decreased a little, and new parameters are reported for cyclopropanes and cyclobutanes. For a CH_2 group in cycloalkanes, σ decreases but ε increases with decreasing ring size. The principal pattern for CH_n groups is that σ decreases in more crowded environments, while ε tends to increase.

The parameters for bond stretching, angle bending, and torsional energetics are given in Table 2. The only changes are the V_1 and V_2 coefficients of the CT−CT−CT−CT torsion decrease from 1.30 and −0.05 kcal/mol in OPLS-AA to 0.85 and −0.20 kcal/mol in OPLS/2020, and for butane, V_1 is set to 1.10 kcal/mol. Butane is also treated uniquely in the CHARMM C27r force field.[10] These changes are needed to bring the force field results into close agreement with the best current estimates for linear alkane conformers.

3.2. Conformational Energetics. Relative conformational energies for alkanes obtained by performing energy minimizations in the gas phase with the OPLS/2020 and OPLS-AA force fields are given in Table 3. The main source of reference data for conformational energetics is the result of high-end quantum-mechanical calculations. There are significant differences depending on the level of ab initio or density functional theory;[32] however, for butane, there is now consensus from CCSD(T) calculations that the *gauche* conformer is 0.60 kcal/mol higher in energy than the *anti* one and that the same difference is obtained for the single *gauche* conformers of pentane and hexane versus the all-*anti* ones.[10,32] The same-sign *gauche* conformers of pentane (*gg*) and hexane (*ggg*) are interesting in that they are only 0.94 and 1.26 kcal/mol higher in energy than *aa* and *aaa*, respectively, while *ca.* 1.20 and 1.80 kcal/mol might have been expected from the single *g*−*a* differences. Thus, there are attractive 1−5 interactions in these conformers, whereas the g^+g^- conformer of pentane shows extra repulsion of 1.6 kcal/mol (2.81−2 × 0.60) for the *syn*-pentane penalty. With the lowering of the *gauche*−*anti* energy difference from 0.8 to 0.9 kcal/mol with OPLS-AA to 0.5−0.6 kcal/mol with OPLS/2020, the conformational energetics for the pentane and hexane conformers are now in close accord with the best available results (Table 3). The first linear alkane for which the all *anti* conformer is not the lowest in energy was also checked.[11] For OPLS/2020, the single hairpin conformer for octadecane is lower in energy than the all *anti* one by 0.55 kcal/mol, which is in good accordance with the CCSD results of *ca.* 1.0 kcal/mol.[42]

https://doi.org/10.1021/acs.jpcb.2c03686
J. Phys. Chem. B 2022, 126, 5896−5907

Table 4. OPLS/2020 Liquid Densities (g/cm^3) for Alkanes Obtained from MC and MD Simulations at 1 atm

molecule	T (°C)	expt.	MC	MD-cutoff	MD-PME
methane	−161.49	0.4239[a]	0.4427	0.4451	0.4602
ethane	−88.63	0.5460[a]	0.5314	0.5423	0.5333
propane	−42.07	0.5810[a]	0.5715	0.5678	0.5730
cyclopropane	−32.8	0.6992[b]	0.6655	0.6646	0.6701
cyclobutane	12.5	0.7100[a]	0.6973	0.6867	0.7022
butane	−0.5	0.6016[a]	0.5864	0.5806	0.5873
butane	25	0.5729[c]	0.5482	0.5417	0.5477
2-methylpropane	25	0.5509[c]	0.5480	0.5392	0.5481
cyclopentane	25	0.7405[c]	0.7137	0.7103	0.7222
pentane	25	0.6214[c]	0.6070	0.6012	0.6052
2-methylbutane	25	0.6142[c]	0.6159	0.6106	0.6138
2,2-dimethylpropane	25	0.5852[c]	0.5937	0.6019	0.5992
cyclohexane	25	0.7739[c]	0.7561	0.7466	0.7572
hexane	25	0.6548[c]	0.6453	0.6387	0.6438
3-methylpentane	25	0.6598[c]	0.6566	0.6546	0.6550
2-methylpentane	25	0.6485[c]	0.6505	0.6483	0.6513
2,3-dimethylbutane	25	0.6570[c]	0.6666	0.6685	0.6651
2,2-dimethylbutane	25	0.6445[c]	0.6558	0.6619	0.6554
heptane	25	0.6795[c]	0.6749	0.6580	0.6715
cyclooctane	25	0.8300[b]	0.8142	0.8167	0.8089
octane	25	0.6986[c]	0.6955	0.6853	0.6929
2,2,4-trimethylpentane	25	0.6878[c]	0.7140	0.7180	0.7124
decane	25	0.7264[c]	0.7271	0.7157	0.7235
dodecane	25	0.7452[c]	ND[d]	0.7362	0.7448
pentadecane	25	0.7650[b]	ND[d]	0.7576	0.7674
hexadecane	25	0.7700[b]	ND[d]	0.7633	0.7733
MAE (%)			1.85	2.39	1.81
MAE			0.0118	0.0155	0.0111

[a]Ref 43. [b]Ref 44. [c]Ref 45. [d]ND = Not Determined.

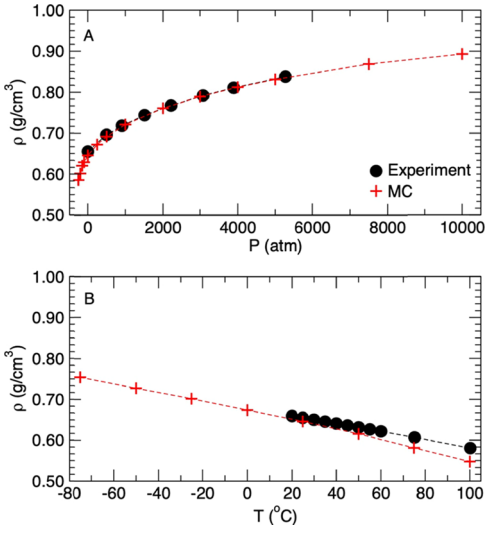

Figure 1. Experimental (Ref 48−50.) and OPLS/2020 densities for liquid hexane from MC simulations as a function of (A) pressure at 25 °C and (B) temperature at 1 atm.

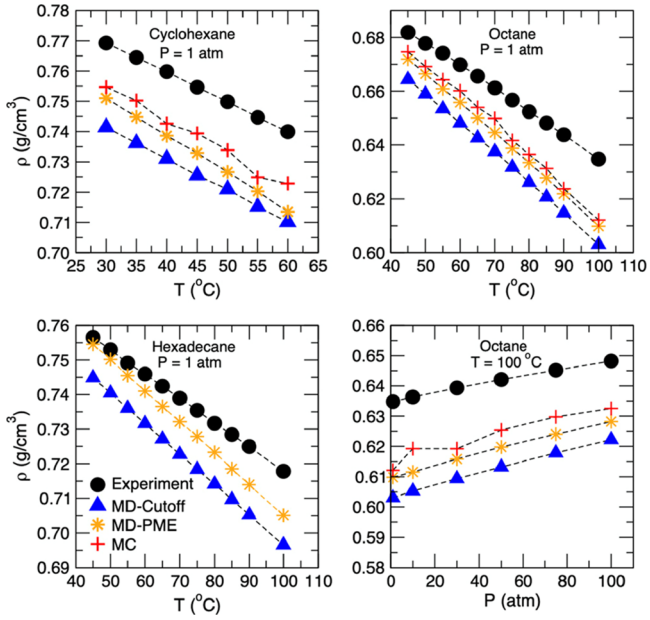

Figure 2. Experimental (Ref 51.) and OPLS/2020 liquid density of cyclohexane, octane, and hexadecane obtained from MD and MC simulations at varying temperatures and pressures.

However, the price to pay is with axial versus equatorial methylcyclohexane, for which the difference is now too small (0.82 kcal/mol) compared to the reference value of 1.76 kcal/mol from both theory and experiment.[35] Similarly, there are underestimates for the higher-energy diastereomers of 1,2-dimethylcyclohexane and decalin.[36,37] These discrepancies could be remedied by declaring a new atom type for an alkyl carbon attached to a cycloalkane, say CX, and assigning the CX−CT−CT−CT torsion term as the same as CT−CT−CT−CT with V_1 changed to 1.40 kcal/mol. This modification should be considered by users for whom high accuracy is needed for the energetics of such systems.

https://doi.org/10.1021/acs.jpcb.2c03686
J. Phys. Chem. B 2022, 126, 5896−5907

Table 5. OPLS/2020 ΔH_{vap} (kcal/mol) for Liquid Alkanes Obtained from MC and MD Simulations at 1 atm

molecule	T (°C)	expt.	MC	MD-cutoff	MD-PME
methane	−161.49	1.957[a]	1.878	1.885	1.905
ethane	−88.63	3.511[a]	3.201	3.306	3.225
propane	−42.07	4.487[a]	4.244	4.150	4.209
cyclopropane	−32.8	4.799[b]	4.716	4.723	4.757
cyclobutane	12.5	5.781[a]	5.609	5.492	5.707
butane	−0.5	5.352[c]	5.049	4.994	5.073
butane	25	5.035[c]	4.719	4.631	4.710
2-methylpropane	25	4.570[c]	4.509	4.371	4.467
cyclopentane	25	6.818[c]	6.350	5.901	5.970
pentane	25	6.316[c]	6.069	5.907	5.985
2-methylbutane	25	5.937[c]	5.851	5.753	5.793
2,2-dimethylpropane	25	5.205[c]	5.077	5.172	5.109
cyclohexane	25	7.861[c]	7.520	7.450	7.519
hexane	25	7.541[c]	7.254	7.102	7.232
3-methylpentane	25	7.236[c]	7.069	7.043	7.049
2-methylpentane	25	7.138[c]	6.977	6.953	7.026
2,3-dimethylbutane	25	6.961[c]	6.878	6.921	6.825
2,2-dimethylbutane	25	6.618[c]	6.482	6.611	6.459
heptane	25	8.736[c]	8.847	8.515	8.706
cyclooctane	25	10.683[d]	10.371	10.240	9.899
octane	25	9.916[c]	9.988	9.494	9.718
2,2,4-trimethylpentane	25	8.401[c]	8.555	8.651	8.505
decane	25	12.277[c]	12.609	11.910	12.221
dodecane	25	14.648[c]	ND[e]	14.328	14.746
pentadecane	25	18.188[d]	ND[e]	18.024	18.625
hexadecane	25	19.431[d]	ND[e]	19.254	19.923
MAE (%)			3.32	3.76	3.14
MAE			0.202	0.257	0.224

[a]Ref 43. [b]Ref 52. [c]Ref 45. [d]Ref 53. [e]ND = Not Determined.

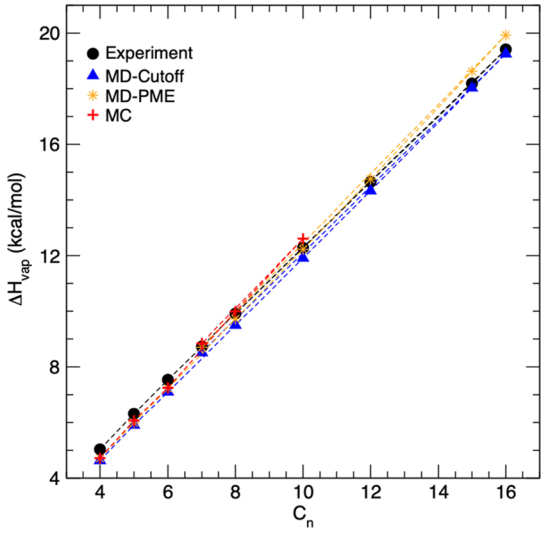

Figure 3. Experimental and OPLS/2020 enthalpies of vaporization vs number of carbons for the normal alkanes obtained from MD and MC simulations at 25 °C and 1 atm.

As a final conformational note, it has been common in the teaching of organic chemistry to assign 0.9 kcal/mol to the *gauche*−*anti* energy difference for butane and then to rationalize the axial−equatorial energy difference of 1.8 kcal/mol, as reflecting the two extra *gauche* relationships in axial methylcyclohexane. This tradition should be abandoned, and rationalization for the extra 0.6 kcal/mol (1.8−2 × 0.6) of strain in axial methylcyclohexane could be sought.

3.3. Thermodynamics of Liquid Alkanes. The OPLS/2020 densities for liquid alkanes are compared with the corresponding experimental values shown in Table 4. The average errors are only 0.01 g/cm^3 or 2%, and there is essentially perfect accordance between the MC and MD-PME results. The MD-cutoff results tend to be slightly lower than the others but within 0.01 g/cm^3. Uncertainties ($\pm 1\sigma$) in the computed values are *ca.* ±0.005 g/cm^3. There is also no drift from the experimental densities with increasing chain length; the MC and MD-PME densities for octane through hexadecane differ from the experimental ones by less than 0.005 g/cm^3 in all cases. The mean-signed error (MSE) in the computed densities varies from −0.004 to −0.008 g/cm^3, indicating that there is no overall bias. However, a compromise was made such that the densities tend to be slightly overestimated for branched alkanes but underestimated for lower linear and cyclic ones.

To study the pressure and temperature dependence of densities, liquid hexane was first examined. The results in Figure 1 with OPLS/2020 show perfect agreement with the experimental data for the pressure dependence at 25 °C up to 5000 atm. This implies that there is no problem with representing the nonbonded interactions in the LJ plus Coulomb format. However, the computed densities drift progressively lower with increasing temperature. The error increases from 1.3% at 25 °C to 4.2% at 75 °C, which is a little above the boiling point at 69 °C. This effect can be attributed to the harmonic treatment of bond stretching and angle bending, which expands the monomers too much with increasing temperature. The force field has been optimized

https://doi.org/10.1021/acs.jpcb.2c03686
J. Phys. Chem. B 2022, 126, 5896−5907

Table 6. Comparison of OPLS-AA and OPLS/2020 Liquid Densities (ρ) and Enthalpies of Vaporization for Alkanes from MC Simulations at 25 °C and 1 atm

	ρ (g/cm^3)			ΔH_{vap} (kcal/mol)		
	expt.	OPLS-AA	OPLS/2020	expt.	OPLS-AA	OPLS/2020
cyclopropane[a]	0.6992[b]	0.6014	0.6655	4.799[b]	3.882	4.716
butane	0.5729[c]	0.5586	0.5482	5.035[c]	5.000	4.719
2-methylpropane	0.5509[c]	0.5609	0.5480	4.570[c]	4.962	4.509
pentane	0.6214[c]	0.6141	0.6070	6.316[c]	6.430	6.069
2,2-dimethylpropane	0.5852[c]	0.6323	0.5937	5.205[c]	6.266	5.077
hexane	0.6548[c]	0.6518	0.6453	7.541[c]	7.888	7.254
3-methylpentane	0.6598[c]	0.6609	0.6566	7.236[c]	7.632	7.069
2-methylpentane	0.6485[c]	0.6566	0.6505	7.138[c]	7.665	6.977
2,3-dimethylbutane	0.6570[c]	0.6706	0.6666	6.961[c]	7.525	6.878
2,2-dimethylbutane	0.6445[c]	0.6734	0.6558	6.618[c]	7.382	6.482
cyclohexane	0.7739[c]	0.7632	0.7561	7.861[c]	8.091	7.520
octane	0.6986[c]	0.6984	0.6955	9.916[c]	10.825	9.988
MAE (%)		3.1134	1.8025		8.304	2.687
MAE		0.0202	0.0117		0.521	0.173

[a] T = −32.8 °C. [b] Ref 52. [c] Ref 45.

Table 7. OPLS/2020 Constant-Pressure Heat Capacities (cal mol^{-1} deg^{-1}) and Isothermal Compressibility Coefficients (atm^{-1}) for Liquid Alkanes Obtained from MC Simulations at 1 atm

			C_p(l)		$10^6\ \kappa$	
molecule	T (°C)	C_p°	MC	expt.	MC	expt.
methane	−161.49	7.96[a]	14.3 ± 0.4		227 ± 12	
ethane	−88.63	9.87[a]	19.2 ± 0.6	17.60[a]	206 ± 12	
propane	−42.07	14.67[a]	24.2 ± 1.2	23.59[b]	198 ± 23	
cyclopropane	−32.8	10.86[a]	20.6 ± 1.0	19.51[c]	140 ± 13	
butane	−0.5	22.05[a]	32.9 ± 0.8	33.40[a]	216 ± 19	
butane	25	23.54[b]	37.9 ± 1.7		379 ± 43	
2-methylpropane	25	23.10[b]	36.2 ± 1.8	33.85[c]	488 ± 62	
cyclobutane	12.6	16.11[d]	26.5 ± 1.3	25.41[d]	142 ± 16	
pentane	25	28.69[b]	40.6 ± 1.0	39.96[b]	204 ± 21	221[b]
2-methylbutane	25	28.41[b]	44.0 ± 1.9	39.55[b]	278 ± 37	248[b]
2,2-dimethylpropane	25	28.88[b]	48.9 ± 4.1		423 ± 98	
cyclopentane	25	19.82[b]	33.5 ± 1.6	31.22[b]	162 ± 29	138[b]
hexane	25	34.08[b]	46.8 ± 1.2	46.72[b]	163 ± 17	173[b]
3-methylpentane	25	33.49[b]	47.1 ± 1.6	45.57[b]	168 ± 17	
2-methylpentane	25	33.99[b]	47.0 ± 1.4	46.35[b]	169 ± 19	
2,3-dimethylbutane	25	33.32[b]	47.9 ± 1.7	45.10[b]	192 ± 23	
2,2-dimethylbutane	25	33.81[b]	45.4 ± 1.8	45.10[b]	179 ± 31	
cyclohexane	25	25.40[b]	39.2 ± 1.6	37.29[b]	110 ± 11	116[b]
heptane	25	39.48[b]	55.2 ± 2.1	53.77[b]	128 ± 15	146[b]
octane	25	44.88[b]	61.3 ± 1.6	60.74[b]	103 ± 7	130[b]
2,2,4-trimethylpentane	25	45.03[b]	61.7 ± 1.8	57.02[b]	146 ± 17	
MAE (%)			4.51		11.49	
MAE			1.61		18.71	

[a] Ref 43. [b] Ref 45. [c] Ref 52. [d] Ref 55.

to give good results for many systems near 25 °C and 1 atm. The only obvious way to accommodate a wider temperature range is to implement temperature-dependent LJ parameters.[46,47]

Liquid density was also computed along the 1 atm isobar for cyclohexane, octane, and hexadecane and along the 100 °C isotherm for octane (Figure 2). The MC and MD-PME results continue to parallel the experimental data well. The mean errors are 2.4, 2.5, and 3.8% for the MC, MD-PME, and MD-Cutoff simulations, respectively, which show a small increase over the mean errors (Table 4). As for hexane, there is a tendency toward increasingly too-low computed densities with increasing temperature. However, the overall accord between the calculated and the experimental liquid densities of alkanes as a function of temperature and pressure is gratifying in view of the static nature of the force field.

Experimental and calculated enthalpies of vaporization (ΔH_{vap}) for liquid alkanes are shown in Table 5. The MC and MD-PME results are again in close accordance with average errors of 0.2 kcal/mol or 3%. The MD-cutoff results are mostly lower and give an average error closer to 4%. The uncertainties in the computed values are ±0.05 kcal/mol. The $\Delta H_{vap}$of normal alkanes increases linearly with the chain length. This trend is perfectly captured with OPLS/2020

https://doi.org/10.1021/acs.jpcb.2c03686
J. Phys. Chem. B 2022, 126, 5896−5907

Table 8. Viscosity η (mPa s) of Liquid Alkanes at 25 °C and 1 atm and the Average Length <L> (Å) of the Cubic Simulation Box

	η	<L>	
	expt.	MD-cutoff	MD-PME
pentane	0.245[a]	47.7	47.6
hexane	0.296[a]	48.6	48.5
heptane	0.382[b]	50.4	50.2
octane	0.511[a]	52.1	51.9
decane	0.840[c]	55.2	55.1
dodecane	1.390[a]	58.1	58.0
pentadecane	2.540[c]	62.1	61.7
hexadecane	3.030[c]	63.2	63.0

[a]Ref 63. [b]Ref 64. [c]Ref 65.

(Figure 3). ΔH_{vap} is slightly underestimated for butane to hexane while slightly overestimated for pentadecane and hexadecane. This reflects much improvement over OPLS-AA, which yields an overly positive slope.[11] Testing so far also indicates that the hydrocarbon parameters for OPLS/2020 can be combined with functional group parameters from OPLS-AA. For example, such treatment of octanol yields a computed density and ΔH_{vap} within 1% of the experimental values at 25 °C and 1 atm.

Further comparison of OPLS-AA and OPLS/2020 is provided in Table 6 for 12 of the smaller alkanes. Giving a higher weight to the description of long-chain hydrocarbons has not worsened the results for shorter linear and branched ones. The mean errors for density and ΔH_{vap} for OPLS/AA of 0.02 g/cm^3 and 0.5 kcal/mol have been reduced to 0.01 g/cm^3 and 0.2 kcal/mol using OPLS/2020, respectively. A goal was to improve the performance for ΔH_{vap} in isomer series. Thus, all the butane, pentane, and hexane isomers were modeled. The problem is compression of the range of computed heats of vaporization compared to experiment. ΔH_{vap} for alkanes decreases with increased branching owing to reduced intermolecular van der Waals attraction with a reduced surface area. For example, the experimental ΔH_{vap} for neopentane (2,2-dimethylpentane) is 1.11 kcal/mol lower than that for pentane, and the difference is 0.92 kcal/mol for hexane and 2,2-dimethylbutane. However, with OPLS-AA, the corresponding differences are 0.16 and 0.51 kcal/mol. These differences are improved to 0.99 and 0.77 kcal/mol with OPLS/2020. The experimental densities for the isomeric series in Table 6 exhibit comparatively little variations; the range for hexanes is only 0.01 g/cm^3. Both force fields also give a small range, 0.02 g/cm^3, for the hexanes, while only OPLS/2020 gives the correct density order for pentane and neopentane, and for butane and isobutane (2-methylpropane). Overall, the results for all alkanes in Table 6 reflect significant improvement with OPLS/2020 over OPLS-AA with decreases in the mean percentage error from 3.1 to 1.8% for liquid densities and from 8.3 to 2.7% for enthalpies of vaporization. For cyclic alkanes versus linear ones with the same number of carbon atoms, the force fields both reproduce the pattern of higher densities and heats of vaporization for the cyclic molecules.

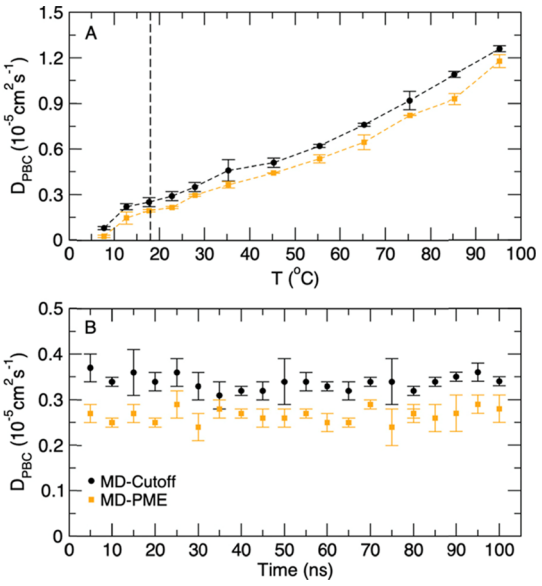

Figure 4. Self-diffusion constants under periodic boundary conditions (D_{PBC}) for liquid hexadecane: (A) as a function of temperature, and (B) as a function of simulation time for the MD runs at 25 °C and 1 atm. Vertical dash line in (A) shows the experimental melting point temperature of hexadecane.

In simulations at constant T and P, both the energy and volume of liquids fluctuate. The associated properties including the heat capacity $C_p(l)$ and the isothermal compressibility coefficient κ converge more slowly than the energy and volume.[54] The calculated values of $C_p(l)$ and κ for liquid alkanes are shown in Table 7 and compared to experimental data where available. The contribution of the intramolecular energy to $C_p(l)$ is taken from the experimental heat capacity of the ideal gas C_p^o (eq 4), which compensates for the classical

Table 9. Self-Diffusion Coefficient D_0 (10^{-5} cm^2 s^{-1}) of Liquid Alkanes at 25 °C and 1 atm (NPT)[a]

	expt.	OPLS/2020		ref[13]	ref[14]
molecule		MD-cutoff	MD-PME	MD	MD
pentane	5.62[b], 5.72[c]	6.201 (5.671)	5.990 (5.459)		
hexane	4.21[d], 4.25[c]	4.463 (4.033)	4.323 (3.892)	3.151	
heptane	3.10[e]	3.218 (2.891)	3.171 (2.843)		
octane	2.36[e]	2.454 (2.220)	2.311 (2.077)		
decane	1.39[e], 1.30[d]	1.415 (1.281)	1.279 (1.145)		
dodecane	0.87[e]	0.823 (0.746)	0.730 (0.653)	0.529	
pentadecane	0.46[e]	0.440 (0.401)	0.374 (0.334)	0.264	0.384
hexadecane	0.39[e]	0.357 (0.325)	0.283 (0.251)		
MSE		0.107 (−0.118)	−0.007 (−0.232)		
MAE		0.157 (0.118)	0.127 (0.232)		

[a]D_{PBC} values are in parentheses. [b]Ref 66. [c]Ref 67, 68. [d]Ref 69. [e]Ref 65.

https://doi.org/10.1021/acs.jpcb.2c03686
J. Phys. Chem. B 2022, 126, 5896−5907

Table 10. OPLS/2020 Hydration Free Energy (kcal/mol) at 25 °C and 1 atm for Alkanes in TIPnP Water Models Obtained from MC and MD-PME Simulations

	expt.	computed					
		TIP3P		TIP4P		TIP5P	
molecule		MC	MD	MC	MD	MC	MD
methane	2.00[a]	2.35	2.34	2.12	2.46	2.46	2.24
ethane	1.83[a]	2.49	2.36	2.02	2.49	2.52	2.18
propane	1.96[a]	2.65	2.47	2.24	2.83	2.83	2.34
butane	2.08[a]	2.97	2.58	2.57	2.93	3.01	2.37
isobutane	2.32[a]	2.76	2.50	2.44	2.83	3.05	2.42
pentane	2.33[a]	3.23	2.76	2.69	3.07	3.26	2.60
2-methylbutane	2.39[b]	3.22	2.63	2.67	3.03	3.30	2.59
2,2-dimethylpropane	2.51[a]	3.20	2.81	2.72	3.05	3.26	2.96
hexane	2.49[a]	3.54	2.89	2.85	3.34	3.50	2.92
cyclohexane	1.23[a]	ND	1.79	ND	2.18	ND	1.75
octane	2.89[a]	ND	3.18	ND	3.79	ND	3.56
cyclopropane	0.75[c]	ND	1.84	ND	2.03	ND	1.72
MAE (9 molecules)		0.72	0.38	0.27	0.66	0.81	0.29
MAE (all molecules)			0.45		0.77		0.41

[a]Ref 70. [b]Ref 71.

treatment of the intramolecular energy with harmonic functions.[54] For the OPLS/2020 results in Table 7, the mean percentage error is 4.6% for $C_p(l)$ and 11.5% for κ.

3.4. Fluidity of Liquid Alkanes. The self-diffusion coefficient, D_0, reflects the fluidity of liquids in the bulk. It has been used for development as well as for cross-benchmark comparison of molecular force fields.[56,57] Nevertheless, it should be stated that D_0 can also be affected by the simulation parameters controlling the kinetics of the system.[58] For instance, thermostating algorithms modify the velocity of the particles enabling simulations to sample the *NVT* ensemble; thus, they alter the dynamics of the system with respect to the *NVE* ensemble.[58,59] The complexity increases when the simulations are conducted in the *NPT* ensemble because barostats also alter the dynamics of the system in order to keep the pressure at a desired value. The implications of such thermostat- and barostat-dependent dynamical artifacts for computer simulations are beyond the scope of this work. However, for validating the OPLS/2020 force field, the effects of stochastic and deterministic thermostats and barostats on the self-diffusion coefficient of liquid alkanes were scrutinized over a range of temperature and pressure coupling constants before settling on the conditions presented in the methods section. The results of these trials indicated that the percentage error in the self-diffusion coefficients computed for liquid pentane, hexane, and octane may vary significantly using different methodologies.

The diffusion coefficient of a liquid simulated under periodic boundary conditions, D_{PBC}, is also system-size-dependent.[17,31] To adjust for this problem, a simple analytical correction was suggested based upon the replacement of the Oseen tensor in the Kirkwood theory of the diffusion constant by the corresponding Ewald summation formula.[17,31] The effect of artifacts imposed by periodic boundary conditions often appears stronger when Ewald-based methods are used rather than cutoff-based ones for treating electrostatic interactions.[60−62] In order to evaluate this effect on the self-diffusion constant, the correction term in eq 6 is added to the D_{PBC} values calculated from both MD-cutoff and MD-PME simulations. Table 8 lists the experimental viscosities of the liquid alkanes and the average length of the simulation box used for the correction in eq 6. The values for D_{PBC} and D_0 are provided in Table 9. When more than one experimental value for D_0 was found, the average is used as the reference value.

Overall, the computed and observed diffusion coefficients are in good agreement, especially for long alkanes. The results with OPLS/2020 show improvements over earlier studies that attempted to refine the OPLS-AA parameters specifically for better fluidity of long hydrocarbon-containing liquids.[14,15] It is apparent from Table 9 that diffusion is lessened in the MD-PME simulations compared to the MD-cutoff ones, although it is only a small effect for these nonpolar liquids. The D_{PBC} correction shown in eq 6 increases diffusion, which increases the error a little for the MD-cutoff results (0.159 vs 0.128 × 10^{-5} cm^2 s^{-1}) and reduces it for the MC-PME results (0.127 vs 0.232 × 10^{-5} cm^2 s^{-1}). Simulations with sequential heating were performed for liquid hexadecane to probe the influence of temperature. Figure 4A shows that D_{PBC} decreases almost linearly as temperature decreases from near 100 to 45 °C while its decrease becomes less linear with further cooling to near 5 °C. One factor may be that with increasing temperature, the population of *gauche*-containing conformers increases, which makes the monomers on-average more compact. At lower temperatures, the higher *anti* populations may make the mechanism of diffusion more complex. In Figure 4B, the D_{PBC} values for liquid hexadecane are plotted as a function of simulation time; the results fluctuate about averages of 0.338 and 0.266 (× 10^{-5} cm^2 s^{-1}) throughout 100 ns with MD-cutoff and MD-PME, respectively. This indicates that liquid hexadecane does not undergo transitions to the gel or the crystalline phase above its melting point (18 °C) in simulations with OPLS/2020, and that the calculated values for the diffusion coefficients are sufficiently converged.

3.5. Hydration Free Energies of Alkanes. The standard TIP*n*P (n = 3, 4, 5) water models[16,29] were used for calculating the hydration free energy of alkanes through MC and MD simulations with the OPLS/2020 force field (Table 10). It should be noted that the long-range electrostatic interactions were treated by the PME algorithm for the MD results reported in Table 10, and a correction for the solute−solvent LJ interactions neglected beyond the cutoff was made in all cases; it ranges from −0.15 to −0.70 kcal/mol upon going

https://doi.org/10.1021/acs.jpcb.2c03686
J. Phys. Chem. B 2022, 126, 5896−5907

from methane to hexane. The uncertainties in the computed values are ±0.2 to ±0.4 kcal/mol. Thus, the differences in the computed results are mostly within the statistical uncertainty and should not be overinterpreted. The MC and MD results agree well, and the average error in comparison to the experimental data is *ca.* 0.5 kcal/mol. There is no clear difference in performance for the three water models. They all reproduce the narrow range of values that is characteristic of the experimental data.[71] There may be a small tendency to make the alkanes too hydrophobic. Further study of this issue is warranted.[72]

4. CONCLUSIONS

The present work provides improved parameters for the OPLS all-atom force field for saturated hydrocarbons, with testing on both branched and long-chain alkanes up to hexadecane. Gas-phase energy minimizations and liquid-phase MC and MD simulations were carried out for validation with computation of gas-phase conformational energetics, liquid properties, and hydration free energies. Results for self-diffusion constants of the liquid normal alkanes exhibited good agreement with the experimental values and showed that long-chain hydrocarbons, such as pentadecane and hexadecane, remain in the fluid phase when simulated with OPLS/2020 above their melting points. Overall, significant improvements are found with OPLS/2020 over OPLS-AA, particularly for long-chain hydrocarbons and for series of linear and branched isomers. The reported parameters can be combined with those for functional groups from the OPLS-AA force field.

AUTHOR INFORMATION

Corresponding Author

William L. Jorgensen − *Department of Chemistry, Yale University, New Haven, Connecticut 06520-8107, United States;* orcid.org/0000-0002-3993-9520; Email: william.jorgensen@yale.edu

Authors

Mohammad M. Ghahremanpour − *Department of Chemistry, Yale University, New Haven, Connecticut 06520-8107, United States;* orcid.org/0000-0002-1129-6041

Julian Tirado-Rives − *Department of Chemistry, Yale University, New Haven, Connecticut 06520-8107, United States;* orcid.org/0000-0001-7330-189X

Complete contact information is available at: https://pubs.acs.org/10.1021/acs.jpcb.2c03686

Notes

The authors declare no competing financial interest.

ACKNOWLEDGMENTS

Gratitude is expressed to the National Institutes of Health (GM032136) for support of this research.

REFERENCES

(1) Allinger, N. L.; Tribble, M. T.; Miller, M. A.; Wertz, D. H. Conformational Analysis. LXIX. Improved Force Field for the Calculation of the Structures and Energies of Hydrocarbons. *J. Am. Chem. Soc.* **1971**, *93*, 1637−1648.

(2) Ryckaert, J.-P.; Bellemans, A. Molecular Dynamics of Liquid Alkanes. *Faraday Discuss. Chem. Soc.* **1978**, *66*, 95−106.

(3) Jorgensen, W. L.; Madura, J. D.; Swenson, C. J. Optimized Intermolecular Potential Functions for Liquid Hydrocarbons. *J. Am. Chem. Soc.* **1984**, *106*, 6638−6646.

(4) Allinger, N. L.; Yuh, Y. H.; Lii, J. H. Molecular Mechanics. The MM3 Force Field for Hydrocarbons. 1. *J. Am. Chem. Soc.* **1989**, *111*, 8551−8566.

(5) Kaminski, G.; Duffy, E. M.; Matsui, T.; Jorgensen, W. L. Free Energies of Hydration and Pure Liquid Properties of Hydrocarbons from the OPLS All-Atom Model. *J. Phys. Chem.* **1994**, *98*, 13077−13082.

(6) Jorgensen, W. L.; Maxwell, D. S.; Tirado-Rives, J. Development and Testing of the OPLS All-Atom Force Field on Conformational Energetics and Properties of Organic Liquids. *J. Am. Chem. Soc.* **1996**, *118*, 11225−11236.

(7) Chen, B.; Siepmann, J. I. Transferable Potentials for Phase Equilibria. 3. Explicit-Hydrogen Description of Normal Alkanes. *J. Phys. Chem. B* **1999**, *103*, 5370−5379.

(8) van Duin, A. C. T.; Dasgupta, S.; Lorant, F.; Goddard, W. A. ReaxFF: A Reactive Force Field for Hydrocarbons. *J. Phys. Chem. A* **2001**, *105*, 9396−9409.

(9) Schuler, L. D.; Daura, X.; van Gunsteren, W. F. An Improved GROMOS96 Force Field for Aliphatic Hydrocarbons in the Condensed Phase. *J. Comput. Chem.* **2001**, *22*, 1205−1218.

(10) Klauda, J. B.; Brooks, B. R.; MacKerell, A. D.; Venable, R. M.; Pastor, R. W. An ab Initio Study on the Torsional Surface of Alkanes and Its Effect on Molecular Simulations of Alkanes and a DPPC Bilayer. *J. Phys. Chem. B* **2005**, *109*, 5300−5311.

(11) Thomas, L. L.; Christakis, T. J.; Jorgensen, W. L. Conformation of Alkanes in the Gas Phase and Pure Liquids. *J. Phys. Chem. B* **2006**, *110*, 21198−21204.

(12) Vorobyov, I. V.; Anisimov, V. M.; MacKerell, A. D., Jr. Polarizable Empirical Force Field for Alkanes Based on Classical Drude Oscillator Model. *J. Phys. Chem. B* **2005**, *109*, 18988−18999.

(13) Leonard, A. N.; Simmonett, A. C.; Pickard, F. C.; Huang, J.; Venable, R. M.; Klauda, J. B.; Brooks, B. R.; Pastor, R. W. Comparison of Additive and Polarizable Models with Explicit Treatment of Long-Range Lennard-Jones Interactions Using Alkane Simulations. *J. Chem. Theory Comput.* **2018**, *14*, 948−958.

(14) Siu, S. W. I.; Pluhackova, K.; Böckmann, R. A. Optimization of the OPLS-AA Force Field for Long Hydrocarbons. *J. Chem. Theory Comput.* **2012**, *8*, 1459−1470.

(15) Murzyn, K.; Bratek, M.; Pasenkiewicz-Gierula, M. Refined OPLS All-Atom Force Field Parameters for *n*-Pentadecane, Methyl Acetate, and Dimethyl Phosphate. *J. Phys. Chem. B* **2013**, *117*, 16388−16396.

(16) Jorgensen, W. L.; Chandrasekhar, J.; Madura, J. D.; Impey, R. W.; Klein, M. L. Comparison of Simple Potential Functions for Simulating Liquid Water. *J. Chem. Phys.* **1983**, *79*, 926−935.

(17) Dünweg, B.; Kremer, K. Molecular Dynamics Simulation of a Polymer Chain in Solution. *J. Chem. Phys.* **1993**, *99*, 6983−6997.

(18) Turupcu, A.; Tirado-Rives, J.; Jorgensen, W. L. Explicit Representation of Cation−π Interactions in Force Fields with $1/r^4$ Nonbonded Terms. *J. Chem. Theory Comput.* **2020**, *16*, 7184−7194.

(19) Jorgensen, W. L.; Tirado-Rives, J. Molecular Modeling of Organic and Biomolecular Systems Using BOSS and MCPRO. *J. Comput. Chem.* **2005**, *26*, 1689−1700.

(20) Jorgensen, W. L.; Thomas, L. L. Perspective on Free-Energy Perturbation Calculations for Chemical Equilibria. *J. Chem. Theory Comput.* **2008**, *4*, 869−876.

(21) Pronk, S.; Páll, S.; Schulz, R.; Larsson, P.; Bjelkmar, P.; Apostolov, R.; Shirts, M. R.; Smith, J. C.; Kasson, P. M.; van der Spoel, D.; Hess, B.; Lindahl, E. GROMACS 4.5: A High-Throughput and Highly Parallel Open Source Molecular Simulation Toolkit. *Bioinformatics* **2013**, *29*, 845−854.

(22) Martínez, L.; Andrade, R.; Birgin, E. G.; Martínez, J. M. PACKMOL: A Package for Building Initial Configurations for Molecular Dynamics Simulations. *J. Comput. Chem.* **2009**, *30*, 2157−2164.

(23) Bussi, G.; Donadio, D.; Parrinello, M. Canonical Sampling through Velocity Rescaling. *J. Chem. Phys.* **2007**, *126*, No. 014101.
(24) Berendsen, H. J. C.; Postma, J. P. M.; van Gunsteren, W. F.; DiNola, A.; Haak, J. R. Molecular Dynamics with Coupling to an External Bath. *J. Chem. Phys.* **1984**, *81*, 3684−3690.
(25) Parrinello, M.; Rahman, A. Polymorphic Transitions in Single Crystals: A New Molecular Dynamics Method. *J. Appl. Phys.* **1981**, *52*, 7182−7190.
(26) Verlet, L. C. "Experiments" on Classical Fluids. I. Thermodynamical Properties of Lennard-Jones Molecules. *Phys. Rev.* **1967**, *159*, 98−103.
(27) Essmann, U.; Perera, L.; Berkowitz, M. L.; Darden, T.; Lee, H.; Pedersen, L. G. A Smooth Particle Mesh Ewald Method. *J. Chem. Phys.* **1995**, *103*, 8577−8593.
(28) Hess, B.; Bekker, H.; Berendsen, H. J. C.; Fraaije, J. G. E. M. LINCS: A Linear Constraint Solver for Molecular Simulations. *J. Comput. Chem.* **1997**, *18*, 1463−1472.
(29) Mahoney, M. W.; Jorgensen, W. L. A Five-Site Model for Liquid Water and the Reproduction of the Density Anomaly by Rigid Nonpolarizable Potential Functions. *J. Chem. Phys.* **2000**, *112*, 8910−8922.
(30) Klimovich, P. V.; Mobley, D. L. A Python Tool to Set up Relative Free Energy Calculations in GROMACS. *J. Comput.-Aided Mol. Des.* **2015**, *29*, 1007−1014.
(31) Yeh, I.-C.; Hummer, G. System-Size Dependence of Diffusion Coefficients and Viscosities from Molecular Dynamics Simulations with Periodic Boundary Conditions. *J. Phys. Chem. B* **2004**, *108*, 15873−15879.
(32) Gruzman, D.; Karton, A.; Martin, J. M. L. Performance of Ab Initio and Density Functional Methods for Conformational Equilibria of $C_nH_{2\ n+2}$ Alkane Isomers (n = 4−8). *J. Phys. Chem. A* **2009**, *113*, 11974−11983.
(33) Pitzer, R. M. The Barrier to Internal Rotation in Ethane. *Acc. Chem. Res.* **1983**, *16*, 207−210.
(34) Churchill, G. B.; Dombrowski, J. P.; Ma, L.; Swana, K.; Bohn, R. K.; Montgomery, J. A. Microwave Spectroscopy and Conformations of 2-Methylbutane and 2,3-Dimethylbutane. *J. Mol. Struct.* **2010**, *978*, 11−13.
(35) Wiberg, K. B.; Hammer, J. D.; Castejon, H.; Bailey, W. F.; DeLeon, E. L.; Jarret, R. M. Conformational Studies in the Cyclohexane Series. 1. Experimental and Computational Investigation of Methyl, Ethyl, Isopropyl, and *Tert*-Butylcyclohexanes. *J. Org. Chem.* **1999**, *64*, 2085−2095.
(36) Klimkowski, V. J.; Manning, J. P.; Schäfer, L. Molecular Structures and Intramolecular Interactions in Dimethyl Cyclohexane Isomers. *J. Comput. Chem.* **1985**, *6*, 570−580.
(37) Egan, C. J. Heat and Free Energy of Formation of the Cis- and Trans-Decalins, Naphthalene and Tetralin, from 298° to 1000° K. *J. Chem. Eng. Data* **1963**, *8*, 532−533.
(38) Ocola, E. J.; Laane, J. Ring-Puckering Potential Energy Functions for Cyclobutane and Related Molecules Based on Refined Kinetic Energy Expansions and Theoretical Calculations. *Chem. Phys.* **2020**, *532*, No. 110647.
(39) Durig, J. R.; Geyer, T. J.; Little, T. S.; Kalasinsky, V. F. Spectra and Structure of Small Ring Compounds. XLVIII. Conformational Stability of Methylcyclobutane from Low Frequency Raman Data of the Gas. *J. Chem. Phys.* **1987**, *86*, 545−551.
(40) Kang, Y. K.; Park, H. S. Puckering Transitions in Cyclohexane: Revisited. *Chem. Phys. Lett.* **2018**, *702*, 82−89.
(41) Wiberg, K. B. The C7−C10 Cycloalkanes Revisited. *J. Org. Chem.* **2003**, *68*, 9322−9329.
(42) Byrd, J. N.; Bartlett, R. J.; Montgomery, J. A. At What Chain Length do Unbranched Alkanes Prefer Folded Conformations? *J. Phys. Chem. A* **2014**, *118*, 1706−1712.
(43) Rossini, F. D. *Selected Values of Physical and Thermodynamic Properties of Hydrocarbons and Related Compounds, Comprising the Tables of the American Petroleum Institute Research Project 44.*; Published for the American Petroleum Institute by Carnegie Press: Pittsburgh, 1953.
(44) Yaws, C. L.; Pike, R. W. *Density of Liquid Organic Compounds*. In Thermodynamical Properties of Chemicals and Hydrocarbons; Elsevier, 2009; pp. 106−197.
(45) Riddick, J. A.; Bunger, W. B.; Sakano, T. K. *Techniques of Chemistry.2: Organic Solvents. Physical Properties and Methods of Purification*, 4th ed.; John Wiley & Sons, Inc., 1986; Vol. 2.
(46) Hohm, U.; Zarkova, L. Extending the Approach of the Temperature-Dependent Potential to the Small Alkanes. *Chem. Phys.* **2004**, *298*, 195−203.
(47) Al-Matar, A. K.; Tobgy, A. H.; Suleiman, I. A. The Phase Diagram of the Lennard-Jones Fluid Using Temperature Dependent Parameters. *Mol. Simul.* **2008**, *34*, 289−294.
(48) Dymond, J. H.; Young, K. J.; Isdale, J. D. Para, Para, *T* Behaviour for n-Hexane + n-Hexadecane in the Range 298 to 373 K and 0.1 to 500 MPa. *J. Chem. Thermodynamics.* **1979**, *11*, 887−895.
(49) Dymond, J. H.; Young, K. J.; Isdale, J. D. Transport Properties of Nonelectrolyte Liquid Mixtures–II. Viscosity Coefficients for the n-Hexane + n-Hexadecane System at Temperatures from 25 to 100 at Pressures Up to the Freezing Pressure or 500 MPa. *Int. J. Thermophys.* **1980**, *1*, 345−373.
(50) Bolotnikov, M. F.; Neruchev, Y. A.; Melikhov, Y. F.; Verveyko, V. N.; Verveyko, M. V. Temperature Dependence of the Speed of Sound, Densities, and Isentropic Compressibilities of Hexane + Hexadecane in the Range of (293.15 to 373.15) K. *J. Chem. Eng. Data* **2005**, *50*, 1095−1098.
(51) Banipal, T. S.; Garg, S. K.; Ahluwalia, J. C. Heat Capacities and Densities of Liquid N-Octane, n-Nonane, n-Decane, and n-Hexadecane at Temperatures from 318.15 K to 373.15 K and at Pressures up to 10 MPa. *J. Chem. Thermodyn.* **1991**, *23*, 923−931.
(52) Yaws, C. L. *Chemical Properties Handbook*, 1st ed.; McGraw Hill, 1999.
(53) *Phase Change Data. NIST Standard Reference Database Number 69*, 2022.
(54) Jorgensen, W. L. Monte Carlo Simulations of Liquids. In *Encyclopedia of Computational Chemistry*; Schleyer, P. V. R., Ed.; Wiley: New York, 1998; Vol. 3, pp. 1754−1763.
(55) Rathjens, G. W.; Gwinn, W. D. Heat Capacities and Entropy of Cyclobutane. *J. Am. Chem. Soc.* **1953**, *75*, 5629−5633.
(56) Pascal, T. A.; Lin, S.-T.; Goddard, W. A., III Thermodynamics of Liquids: Standard Molar Entropies and Heat Capacities of Common Solvents from 2PT Molecular Dynamics. *Phys. Chem. Chem. Phys.* **2011**, *13*, 169−181.
(57) Wang, J.; Hou, T. Application of Molecular Dynamics in Molecular Property Prediction II: Diffusion Coefficient. *J. Comput. Chem.* **2011**, *32*, 3505−3519.
(58) Koopman, E. A.; Lowe, C. P. Advantages of a Lowe-Andersen Thermostat in Molecular Dynamics Simulations. *J. Chem. Phys.* **2006**, *124*, 204103.
(59) Basconi, J. E.; Shirts, M. R. Effects of Temperature Control Algorithms on Transport Properties and Kinetics in Molecular Dynamics Simulations. *J. Chem. Theory Comput.* **2013**, *9*, 2887−2899.
(60) Figueirido, F.; Del Buono, G. S.; Levy, R. M. On Finite-size Effects in Computer Simulations Using the Ewald Potential. *J. Chem. Phys.* **1995**, *103*, 6133−6142.
(61) Sakane, S.; Ashbaugh, H. S.; Wood, R. H. Continuum Corrections to the Polarization and Thermodynamic Properties of Ewald Sum Simulations for Ions and Ion Pairs at Infinite Dilution. *J. Phys. Chem. B* **1998**, *102*, 5673−5682.
(62) Weber, W.; Hünenberger, P. H.; McCammon, J. A. Molecular Dynamics Simulations of a Polyalanine Octapeptide under Ewald Boundary Conditions: Influence of Artificial Periodicity on Peptide Conformation. *J. Phys. Chem. B* **2000**, *104*, 3668−3675.
(63) Yaws, C. L. *Yaws' Critical Property Data for Chemical Engineers and Chemists*; Knovel, 2012.
(64) Michailidou, E. K.; Assael, M. J.; Huber, M. L.; Abdulagatov, I. M.; Perkins, R. A. Reference Correlation of the Viscosity of *n*-Heptane from the Triple Point to 600 K and up to 248 MPa. *J. Phys. Chem. Ref. Data* **2014**, *43*, No. 023103.

https://doi.org/10.1021/acs.jpcb.2c03686
J. Phys. Chem. B 2022, 126, 5896−5907

(65) Tofts, P. S.; Lloyd, D.; Clark, C. A.; Barker, G. J.; Parker, G. J. M.; McConville, P.; Baldock, C.; Pope, J. M. Test Liquids for Quantitative MRI Measurements of Self-diffusion Coefficient in Vivo. *Magn. Reson. Med.* **2000**, *43*, 368−374.
(66) Fishman, E. Self-Diffusion in Liquid Normal Pentane and Normal Heptane. *J. Phys. Chem.* **1955**, *59*, 469−472.
(67) Holz, M.; Weingartner, H. Calibration in Accurate Spin-Echo Self-Diffusion Measurements Using 1H and Less-Common Nuclei. *J. Magn. Reson.* **1969**, *1991*, 115−125.
(68) Price, W. S.; Söderman, O. Self-Diffusion Coefficients of Some Hydrocarbons in Water: Measurements and Scaling Relations. *J. Phys. Chem. A* **2000**, *104*, 5892−5894.
(69) McCall, D. W.; Douglass, D. C.; Anderson, E. W. Self-Diffusion in Liquids: Paraffin Hydrocarbons. *Phys. Fluids* **1959**, *2*, 87−91.
(70) Marenich, A. V., Kelly, C. P., Thompson, J. D., Hawkins, G. D., Chambers, C. C., Giesen, D. J., Winget, P., Cramer, C. J., Truhlar, D. G. *Minnesota Solvation Database (MNSOL) Version 2012*.
(71) Mobley, D. L.; Guthrie, J. P. FreeSolv: A Database of Experimental and Calculated Hydration Free Energies, with Input Files. *J. Comput.-Aided Mol. Des.* **2014**, *28*, 711−720.
(72) Piana, S.; Donchev, A. G.; Robustelli, P.; Shaw, D. E. Water Dispersion Interactions Strongly Influence Simulated Structural Properties of Disordered Protein States. *J. Phys. Chem. B* **2015**, *119*, 5113−5123.

https://doi.org/10.1021/acs.jpcb.2c03686
J. Phys. Chem. B 2022, 126, 5896−5907